Fracture Mechanics Analysis Related to Electromagnetic Force

T. Horie, G. Yagawa, Y. Ando
Department of Nuclear Engineering,
University of Tokyo, 3-1 Hongo, 7-chome, Bunkyo-ku, Tokyo 113, Japan
M. Masuda
Japan Atomic Energy Research Institute, Tokai-mura, Ibaraki, Japan

SUMMARY

In most of the conceptual designs of Tokamak fusion power reactors, high magnetic field (several Teslas) is required to confine the plasma. For this purpose, superconducting magnets are considered to be employed as toroidal field coils. In this case the interaction between the magnetic field and the electric current in the coil causes a huge amount of magnetic force which is applied to the structural materials of the coils. In other components of the fusion reactor, especially in the first wall, the magnetic force will occur due to the interaction of the induced current and the magnetic field. Therefore, the effects of electromagnetic loading on the structures of the fusion reactor need to be clarified when fusion reactors are designed or actually constructed. Especially, fracture phenomena of the toroidal field coils may be one of the most critical problems in fusion reactor design because enormous electric energy will be stored in the coils.

This paper is concerned with both numerical analysis and experiment on the fracture phenomena related to the electromagnetic force. We consider a simple model of a single edge cracked beam carrying transient current I and set in a uniform and steady magnetic field B. As the results of their interaction, dynamic electromagnetic force, i.e. I×B, occurs in the beam and it deforms in the opening mode of the crack tip and then fracture is expected to occur. The present analysis consists of two parts. One is the determination of the current distribution in the structures and the other is that of the time variation of a fracture mechanics parameter such as the stress intensity factor or the J-integral caused by the dynamic electromagnetic force.

Performing a 2-dimensional dynamic crack analysis for an aluminum alloy beam, we obtain time variation of the stress intensity factor using isoparametric quarter point elements to predict crack initiation time. As the current density has the same singularity at the crack tip as that of the stress distribution, we also use the quarter point elements in the current density analysis. In the experiment, the crack initiation time, the clip gage displacement and the deflection at the center of the beam are measured.

The unstable fracture may be a critical problem for fusion reactors because of the character of the electromagnetic force, we perform a calculation on the post-yield fracture parameters regarding the cracked structure under the electromagnetic force.

1. Introduction

In most of the conceptual designs of Tokamak fusion power reactors, high magnetic field of several Teslas generated by superconducting magnets is required for the plasma confinement. In this case the interaction between the magnetic field and the electric current in the structures causes a huge amount of magnetic force, which works on the structural components. Therefore, the effects of electromagnetic loading on the structures need to be clarified when fusion reactors are designed or actually constructed. Especially, fracture phenomena of the fusion reactor structures [1-4] may be one of the most critical problems.

This paper is concerned with both numerical analysis and experiment on the fracture phenomena related to the electromagnetic force, considering a simple model of edge cracked beam shown in Fig. 1, which carries transient current I and is set in a uniform and steady magnetic field B_0. The electromagnetic body force (Lorentz force) given by the cross product $I \times B_0$ will be generated in the structure and the beam deforms in (-y) direction, which corresponds to the crack opening direction.

2. Numerical Analysis

2.1 Analysis of Current Density Distribution

It is obvious from Fig. 1 that the electric current does not flow uniformly in the test specimen due to crack effect but it turns around the crack tip. Therefore, in order to obtain electromagnetic force accurately, it is necessary to know the current density distribution in x-y plane of the cracked beam.

Neglecting the skin effect of current density, the equation of continuity, the current density $\vec{i}$, and the electric field $\vec{E}$ are written as

$$\vec{\nabla} \cdot \vec{i} = 0 \quad (1), \qquad \vec{i} = \kappa \vec{E} \quad (2), \qquad \vec{E} = -\vec{\nabla}\phi \quad (3)$$

where κ and ϕ are the electrical conductivity and the electrostatic potential, respectively. The substitution of Eqs.(2) and (3) into Eq.(1) leads to Laplace's equation

$$\vec{\nabla}^2 \phi = 0 \qquad (4)$$

where the electrical conductivity is assumed to be constant over the domain considered. The current distribution can be calculated solving Eq.(4) with Eqs.(2) and (3).

The singularity of the current density distribution at the vicinity of the crack tip is much the same as that of the elastic stress field, which can be derived from the analogy with anti-plane shearing mode singular stress distribution obtained also from the Laplace's equation, i.e.

$$i_r = \frac{L}{\sqrt{2\pi r}} \sin\frac{\theta}{2}, \qquad i_\theta = \frac{L}{\sqrt{2\pi r}} \cos\frac{\theta}{2} \qquad (5a), (5b)$$

at the vicinity of the crack tip, where (r,θ) represents the polar coordinates centered at the crack tip and L is a parameter that represents the concentration of the current density, which is analogous to the stress intensity factor in the linear fracture mechanics.

We use the eight-noded isoparametric element with mid-side nodes at the quarter points [5,6] to calculate the current density distribution. The calculated current density distribution around the crack is shown in Fig. 2, where ϕ=0.2V is given on the left end as a boundary condition, ϕ=0V on the crack prolongation line as a symmetric condition, and $\kappa = 3.5 \times 10^7 / \Omega m$. It can be seen that the electric current flows turning around the crack tip and that the amplitude of the current density increases near the crack tip.

2.2 Analysis of Linear Fracture Mechanics

Calculate the time variation of the stress intensity factor for the test specimen shown in Fig. 1 in which the dynamic electromagnetic force is applied. Although various methods have been developed for stress intensity factor determination using the finite element analyses, we use the quarter point isoparametric element technique [5,6] which is easily applicable to the dynamic case. The transient electric current conducting in the specimen is assumed as shown in Fig. 3. Further, we assume that the applied magnetic field is uniform and steady and that the magnetic field induced by the conducting current itself and the skin effect of electric current are negligible.

The input data for this analysis are as follows: B_0=0.85T, E(=Young's modulus)=7.19×10^{10}N/m^2, ν(=Poisson's ratio)=0.27, ρ(=mass density)=2.88×10^3kg/m^3, and Δt(=time increment)=4×10^{-5}sec. Figure 4 shows the calculated time history of the stress intensity factor. Although the peak value of the loading is set at about 0.6 msec as shown in Fig. 3, that of the stress intensity factor occurs at 3 msec. This time lag is due to the inertia effect. It can be seen from Fig. 4 that the stress intensity factor exceeds the fracture toughness of the material (K_{IC}=22MN/m$^{3/2}$) and the crack initiation will occur at 1.6 msec.

3. Experiment

3.1 Test Specimen

Mechanical notch was machined in the test specimens which were made of aluminum alloy 7178 T-6 and fatigue crack was given till the length of a/W=0.5 (a: crack length, W: width of test specimen). Independently, the fracture toughness K_{IC} of the material was determined based on the ASTM standard E399-74. As the temperature dependence of fracture toughness was observed relatively small, we take the fracture toughness to be 22MN/m$^{3/2}$.

3.2 Main Electric Circuit

Figure 5 shows the main electric circuit which gives the transient electric current in the specimen. Between the terminals A and B, alternating current is supplied. Electric charge is stored in main condenser (22mF) and then discharged when the circuit is closed. SCR (Silicon Controlled Rectifier) is used as a noiseless switch, which starts to work when the trigger pulse is supplied between the terminals G and K. Circuit constants was estimated from the electric current profile as L≃7 μH and R≃50mΩ, where L and R are inductance and resistance, respectively.

3.3 Measurements

We have made the following measurements during each test, (1) Electric current profile, (2) central deflection of the test specimen, (3) crack opening displacement, and (4) strain at the vicinity of the crack tip. Tests were carried out varying the charging voltage of main condenser V_c, and detailed results of tests are given in [4]. Figure 6 shows the time variations of the deflection and the current when V_c is 200V. In the middle of the deflection curve we can see the flat part, which may correspond to the initiation of crack propagation. We define the crack initiation time estimated from the flat part of the deflection curve as t_f^{δ} and that from the break of the strain gage as t_f^{s}. Figure 7 shows the relation of the fracture time versus the charged voltage of the main condenser and the results of the finite element analysis. It can be seen from this figure that the experimental results are slightly higher than those of the finite element method. This

discrepancy may be due to the time lag of the break of the strain gage because of the effect of shear lips which was observed on fracture surfaces after experiments.

As shown in Fig. 6, the electric current kept flowing even after the crack initiation occurred and the electromagnetic force acts as dead load. There is the possibility of unstable fracture [7,8] even for ductile materials, and this characteristic of electromagnetic force would cause a critical problem in the fusion reactor design.

4. Some Discussions

4.1 Consideration of Nonlinear Fracture Mechanics

In several designs of blankets and superconducting toroidal field coils, ductile materials such as 304 s.s. and 316 s.s. are selected as structural materials [9]. Here, we analyze the edge cracked specimen made of a ductile material based on the nonlinear fracture mechanics. The specimen geometry is the same as that shown in Fig. 1 except the thickness and the width which are 9mm and 20mm, respectively.

As a fracture mechanics parameter, we adopt the extended J-integral with the effect of body force [10], which can be written for our case as

$$J=\int_{\Gamma}(Wn_1-T_i\frac{\partial u_i}{\partial x_1})d\Gamma+\int_A\{\rho\ddot{u}_i-(\vec{i}\times\vec{B})_i\}\frac{\partial u_i}{\partial x_1}dA \qquad (6)$$

where T_i is the traction force along the path Γ, and $W,\vec{n},\vec{u},\rho$ and A are the strain energy density, the unit normal vector, the displacement, the mass density and the domain surrounded by Γ, respectively. Figure 8 shows the integration paths Γ.

Performed is the dynamic elasto-plastic analysis, where we assume that the electric current flows as shown in Fig. 9 and that the magnetic induction field $\vec{B}$ is 2 Teslas. Material properties adopted are those of 304 s.s.. Figure 9 also shows the calculated time variation of the J-integral. In Fig. 10, we give the relations of the J-integral vs. integral path showing that the path independency of the present J-integral is satisfied well.

4.2 Analysis of Skin Effect of the Electric Current

In subsection 2.1 we have neglected the skin effect of the electric current in the analysis, which allow us to treat the problem as two dimensional one. Since the current density has the distribution in thickness direction by the skin effect, the current density distribution in y-z plane shown in Fig. 1 is in fact significant.

Neglecting the displacement current, the Maxwell's equations are reduced to

$$\nabla\times\vec{H}=\vec{i}\ , \qquad (7)$$

$$\nabla\times\vec{E}=-\frac{\partial\vec{B}}{\partial t} \qquad (8)$$

where $\vec{H}$ and $\vec{B}$ are the magnetic field intensity and the magnetic induction field, respectively. The constitutive equation connecting $\vec{H}$ to $\vec{B}$ is

$$\vec{B}=\mu\vec{H} \qquad (9)$$

where μ is the magnetic permeability. Since the magnetic induction field $\vec{B}$ can be derived from the vector potential $\vec{A}$ by the relation

$$\vec{B}=\nabla\times\vec{A} \qquad (10)$$

Eq. (8) becomes

$$\vec{E} = -\nabla\phi = \frac{\partial \vec{A}}{\partial t} . \qquad (11)$$

From Eqs. (2),(7),(9),(10), and (11), the differential equation for $\vec{A}$ can be derived as

$$\vec{\nabla}\times\vec{\nabla}\times\vec{A} = \mu\kappa(-\vec{\nabla}\phi - \frac{\partial \vec{A}}{\partial t}) . \qquad (12)$$

Assuming that the electric current flows only in x direction in Fig. 1 and that two dimensional problem in the y-z plane is considered, the vector potential $\vec{A}$ has the x component only. Thus, Eq. (12) simply becomes

$$(\frac{\partial^2}{\partial y^2} + \frac{\partial^2}{\partial z^2})A_x + \mu i_0 = \mu\kappa\frac{\partial A_x}{\partial t} \qquad (13)$$

where $$i_0 \equiv -\kappa\frac{\partial \phi}{\partial x} . \qquad (14)$$

Equation (13) can be discretized with Galerkin's method in space and with Crank-Nicolson's formula in time.

Since we have to give the value of vector potential at infinity as a boundary condition, boundary element method [11] is employed in this paper. Especially, it is readily applicable because Eq. (13) can be reduced to Laplace's equation in the air where the electrical conductivity vanishes.

The finite element equation for the region of the conductor can be written as

$$[K]\{A_x\} + [C]\frac{\partial}{\partial t}\{A_x\} + \{F\} = [E]\{\frac{\partial A_x}{\partial n}\} \qquad (15)$$

where $\frac{\partial}{\partial n}$ is the normal derivative. The boundary element method is applied to the outer region of the conductor or the region of air, and the equation can be written as

$$[H]\{A_x\} = [G]\{\frac{\partial A_x}{\partial n}\} . \qquad (16)$$

Here, A_x and $\partial A_x/\partial n$ are values on the boundary between the inner and outer regions. Substituting Eq. (16) into Eq. (15) so as to eliminate the term of $\partial A_x/\partial n$ or link the two regions, we obtain the equation to be solved.

Because of the geometrical symmetry, the quarter of the conductor region is subdivided into finite elements, but whole boundary between the conductor and air is subdivided into boundary elements as shown in Fig. 11. Therefore, we link the two regions with additional conditions of (see Fig. 12)

$$\{A_x\}_1 = \{A_x\}_2 = \{A_x\}_3 = \{A_x\}_4 . \qquad (17)$$

Assume the value of i_0 as shown in Fig. 3, and the material properties to be $\mu_{al} = \mu_{air} = 1.257\times10^{-6}$H/m, $\kappa_{al} = 3.5\times10^7/\Omega$m, and $\kappa_{air} = 0/\Omega$m. The calculated current density distribution is shown in Fig. 13. It can be seen from this figure that the skin effect is considerable at the earlier time.

5. Conclusions

Experiment and numerical analysis were carried out on the dynamic fracture of edge cracked specimen under the electromagnetic force.

Some discussions were given in view of the nonlinear fracture mechanics and the skin effect of electric current.

Acknowledgement

The work reported in this paper was performed with a financial support from the

Controlled Thermonuclear Reactor Committee, the University of Tokyo.

References

[1] REICH, M., POWELL, J.R., "Generic Structural Mechanics Aspects of Fusion Magnet Systems", Nuclear Engineering and Design, Vol. 58, p. 145, 1980.

[2] CRAMER, B.A., DAVIS, J.W., "Fracture Mechanics Issues for Irradiated Blanket structures", Nuclear Engineering and Design, Vol. 58, p. 267, 1980.

[3] NICKELL, R.E., ESZTEGAR, E.P., "Development of Fatigue Criteria for Experimental Fusion Reactor First-Wall Structures", Nuclear Engineering and Design, Vol. 58, p. 283, 1980.

[4] YAGAWA, G., MASUDA, M., HORIE, T., ANDO, Y., "Dynamic Fracture of Cracked Beam under Electromagnetic Force", paper presented at International Conference on Analytical and Experimental Fracture Mechanics, Rome, Italy, 23-27 June 1980.

[5] HENSHELL, R.D., SHAW, K.G., "Crack Tip Finite Elements Are Unnecessary", Int. Journal for numerical Methods in Engineering, Vol. 9, p. 495, 1975.

[6] BARSOUM, R.S., "On the Use of Isoparametric Finite Elements in Linear Fracture Mechanics", Int. Journal for Numerical Methods in Engineering, Vol. 10, p. 25, 1976.

[7] PARIS, P.C., TADA, H., ZAHOOR, A., ERNST, H., "The Theory of Instability of the Tearing Mode of Elastic-Plastic Crack Growth", ASTM STP 668, p. 5, 1979.

[8] HUTCHINSON, J.W., PARIS. P.C., "Stability Analysis of J-Controlled Crack Growth", ASTM STP 668, p. 37, 1979.

[9] McHENRY, H.I., REED, R.P., "Structural Alloys for Superconducting Magnets in Fusion Energy Systems", Nuclear Engineering and Design, Vol. 58, p. 219, 1980.

[10] KISHIMOTO, K., AOKI, S., SAKATA, M., Transactions of the Japan Society of Mechanical Engineers, Vol. 46, p. 1049, 1980 (in Japanese).

[11] BREBBIA, C. A., "The Boundary Element Method for Engineers", 1978, Pentech Press.

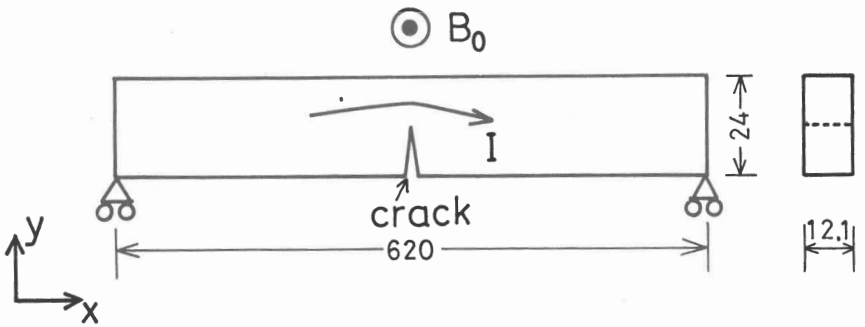

Fig. 1 Edge cracked beam under electromagnetic force.

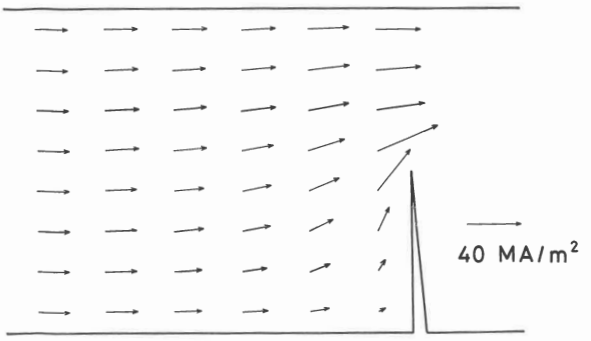

Fig. 2 Electric current density distribution near the crack tip.

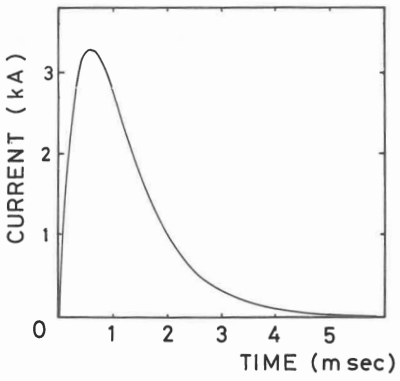

Fig. 3 Time variation of electric current I.

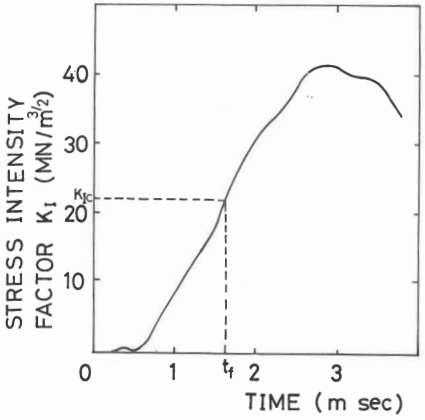

Fig. 4 Calculated time variation of stress intensity factor K_I.

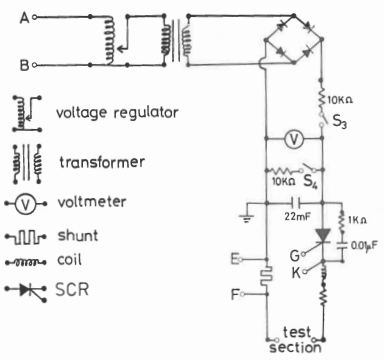

Fig. 5 Main electric circuit.

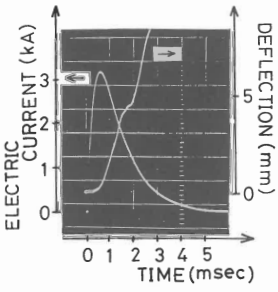

Fig. 6 Electric current and deflection vs. time.

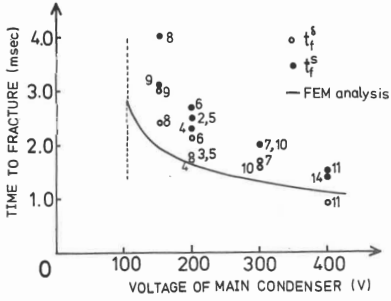

Fig. 7 Time to fracture vs. voltage of main condenser.

Fig. 8 Paths for J-integral calculation.

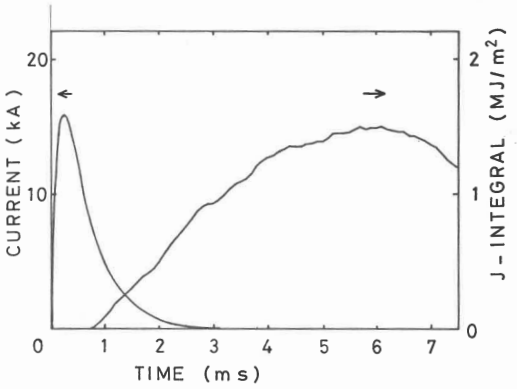

Fig. 9 Time variation of electric current and calculated J-integral for ductile material.

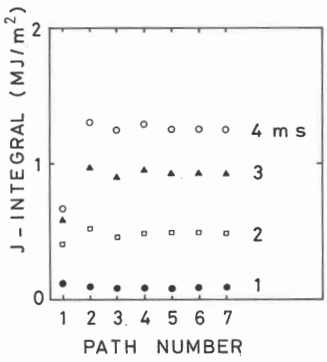

Fig. 10 Path independency of calculated J-integral at each time step.

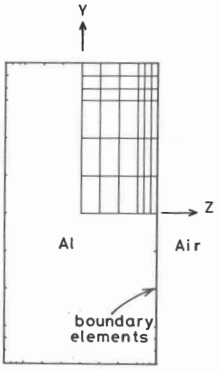

Fig. 11 Finite elements for the conductor and boundary elements for the air.

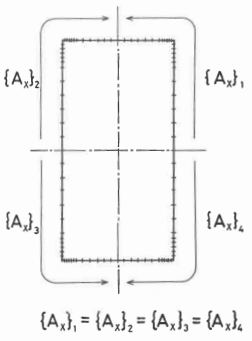

Fig. 12 Additional conditions for connecting finite elements and boundary elements.

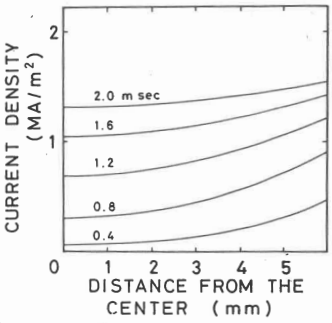

Fig. 13 Calculated current density distribution in thickness direction.